White Paper

Numerical Studies of Wind Turbine Acoustics

Modern industrial economies are heavily reliant on electricity. As a result, developing and maintaining a sufficient supply of affordable and reliable power is a priority for every nation. At the same time, a number of factors have combined to stimulate increased interest in more "environmentally friendly" methods of power generation, such as wind or solar. With the currently ongoing political turmoil in the Middle East and the recent Fukushima nuclear accident, this interest is only increasing.

Introduction

Innovative Technology Applications Company, LLC (ITAC) is currently working as part of an Illinois Institute of Technology (IIT) led team to investigate various aspects of wind power generation. ITAC's portion of this work involves the numerical simulation of the flow around wind turbines and investigating the acoustic field associated with the unsteady fluid behavior.

The current paper discusses the progress made in this work, the analysis methods used, and the results obtained.

Numerical Methods

The current methodology combines the abilities of three different numerical tools to predict the unsteady flow around a wind turbine, the resulting acoustics, and an analysis of the noise sources. The Navier-Stokes equations are solved using the OVERFLOW solver to obtain an unsteady flow field in the vicinity of the turbine. Data from this solution is then fed into the PSU-WOPWOP Ffowcs-Williams Hawkings solver to predict the farfield acoustics. This prediction is used to record sound levels at virtual microphone locations, and this information is fed into the Beamform Interactive software package which is used to analyze the data using a variety of beamforming methods.

This methodology is referred to as the "synthetic array technique" as it uses numerical methods to perform an analysis identical to that used for experimental data from microphone arrays. A similar technique was successfully used in a previous joint effort by ITAC, Dr. Dougherty, and Profs. Brentner and Morris for the acoustics of an airfoil with a blunt trailing edge.

The OVERFLOW Flow Solver

The CFD code used for this work was version 2.2 of the OVERFLOW solver, which is the latest release of this widely used code from NASA Langley1 2. This software is a state-of-the-art Navier-Stokes solver for structured meshes. The original OVERFLOW code has long been used successfully for a wide variety of Reynolds-averaged Navier-Stokes (RANS) simulations3 4 5. Recent additions to the code make it particularly attractive for the work reported here 6 7 8.

OVERFLOW 2.2 solves the time-dependent Navier-Stokes equations in an implicit manner on overset structured meshes. The compressible form of the equations are solved in conservative form on a curvilinear coordinate system.

The current work made use of the "OVERFLOW-D mode" (originally from the code of the same name by Robert Meakin). Compared to the regular mode of operation, this option requires some additional input files and NAMELIST input, but it enables is the use of internal mesh assembly algorithms (called "Domain Connectivity Function"—DCF) for simulations with moving meshes. This obviates the need for an external mesh assembly package (such as PEGSUS or SUGGAR).

© 2018 Tecplot, Inc. All rights reserved worldwide. Tecplot®, Tecplot 360™ and the Tecplot 360™ Logo are registered trademarks and "Master the View™" is a trademark of Tecplot, Inc., Bellevue, WA, USA. All other trademarks are the property of their respective owners.

We also made use of the OVERFLOW-D mode capability for automatic off-body mesh generation. When used in this fashion, Cartesian outer meshes can be automatically generated prior to mesh assembly using DCF. Only the near-body meshes must be provided to the code by the user.

Similar to OVERFLOW-D mode, OVERFLOW now has a built-in 6-DOF (six degree-of- freedom) mesh motion module called the "Geometry Manipulation Protocol" (GMP). GMP is a protocol for specifying geometric hierarchies and associated rigid-body motion. OVERFLOW currently implements only a subset of the larger GMP, but this capability is more than sufficient for the current work, and eliminates the need for an external mesh motion package.

Another extremely useful capability of the OVERFLOW solver is Adaptive Mesh Refinement (AMR). This is the ability to adapt the off-body Cartesian meshes (generated using the OVERFLOW-D mode discussed above) to better resolve the propagation of flow features away from the near-body meshes. The initial off-body Cartesian mesh generation algorithm produces a multi-block configuration where the blocks surrounding the near-body meshes closely match the resolution of those near-body meshes. Away from the near-body meshes, however, the resolution becomes extremely coarse.

The initial configuration is perfectly suitable for starting the simulation, but as the run progresses, the vortices shed from the rotor (as well as from the nacelle and tower) will be dissipated due to the lack of mesh resolution unless the computational mesh is refined in the necessary regions. Likewise, because the rotor is constantly sweeping through space, there may be regions which at one time require refinement, but which later do not need it.

The traditional approach to such a situation is to generate a mesh which is refined everywhere that might ever need such refinement throughout the entire simulation. This typically results in a huge mesh (in terms of number of points). Furthermore, such meshes almost always have one of two significant drawbacks. In the first case, the flow features of interest do not always move exactly as expected, and thus some may move beyond the refined region of the mesh (and thus fail to propagate correctly). In the other case, meshes are often over-refined, or finely spaced in regions which do not need them. This results in a significantly increased run time for the simulation.

OVERFLOW's mesh adaption algorithm allows the off-body mesh to be refined and/or coarsened as the solution progresses. Our initial wind turbine simulations did not employ the adaptive mesh refinement algorithm, and a consequence of this was that the unsteady features in the flow were largely dissipated once they had propagated more than one radius downstream.

The results reported here did use the AMR algorithm, and because of this, the unsteady flow features were successfully propagated much further downstream. For the current work, vorticity magnitude was used to trigger the adaption sensor. Mesh refinement was performed every 40 time steps for the cases reported here, which corresponds to every five degrees of rotation of the rotor.

One drawback of the AMR algorithm is that, while it is more efficient than refining the mesh everywhere, it still results in a significant increase in mesh size. In this case, the baseline mesh had approximately 30.5 million points, but with AMR, the runs reported here ultimately used meshes which had more than 260 million points on any given time step.

The solver was run with a second order implicit scheme in time in conjunction with a dual time marching method to obtain a time-accurate solution. Six sub-iterations per time step were used to synchronize the boundaries with the interior flow and better allow for signals to propagate between computational mesh blocks.

A second order central difference method was used for the explicit convective terms on the near- body meshes, with spectral-radius based smoothing to prevent spurious oscillations. For the off- body meshes, both AMR and a 4th order central scheme were used, along with a higher-order filter to prevent the build-up of spurious oscillations. Since the majority of the flow domain contains very low speed flow (compared to the typical aircraft external flow situations for which OVERFLOW was originally designed), a Low Mach number preconditioning algorithm was also used to stabilize the code.

A Delayed Detached Eddy Simulation version of the SST turbulence model was used in the near- body meshes, but the off-body meshes were run inviscid. The turbulence model convective terms were solved second order.

© 2018 Tecplot, Inc. All rights reserved worldwide. Tecplot®, Tecplot 360™ and the Tecplot 360™ Logo are registered trademarks and "Master the View™" is a trademark of Tecplot, Inc., Bellevue, WA, USA. All other trademarks are the property of their respective owners.

The PSU-WOPWOP Noise Prediction Code

Theoretical Background

The PSU-WOPWOP code is based on the concept of an acoustic analogy. The acoustic analogy was introduced by Lighthill9 in his seminal paper on sound generated aerodynamically. In an acoustic analogy the equations of motion are rearranged into the form of a wave propagator and equivalent sources. This pioneering work introduced the concept of convective amplification and Doppler frequency shift.

Lilley[10] introduced an acoustic analogy in which the wave propagator included the effects of mean shear and density gradients. In the case of a parallel shear flow the equivalent sources are all at least second order in the turbulent fluctuations. Noise prediction methods based on Lilley's equation generally use steady calculations of the flow development, such as provided by a RANS-based Navier-Stokes solver. These are used to set the length and time scales of the turbulence. Examples include methods for jets developed by Khavaran et al.[11] and Khavaran[12].

In their 1969 paper, Ffowcs Williams and Hawkings[13] utilized the powerful technique of generalized function theory to an extension to the Lighthill acoustic analogy that enabled them to consider the noise generated by surfaces in arbitrary motion. The FW–H equation is an exact rearrangement of the continuity equation and the Navier–Stokes equations into the form of an inhomogeneous wave equation with two surface source terms (monopole and dipole) and a volume source term (quadrupole). Although the quadrupole source contribution is insignificant in many subsonic applications with solid surfaces, it is the only noise source term in the original Lighthill acoustic analogy and is particularly relevant for jet noise. Even so, the quadrupole source term in the FW–H equation is a volume source term, therefore it is considerably more expensive to evaluate than the surface source terms.

Although originally pointed out by Ffowcs Williams and Hawkings, the usefulness of the FW–H equation as a Kirchhoff type equation was demonstrated by Brentner and Farassat14. In this application, the fictitious surface used in the derivation of the FW–H is located not on a solid body, as in the classical implementation, but rather surrounding all the relevant noise sources. Thus the integration surface (or acoustic data surface) is a fictitious surface (like a control volume) located in the fluid; hence, this application of the FW–H is called the permeable (or porous) surface formulation because fluid may flow through the surface. With all the significant acoustic sources contained inside the surface, the volume quadrupole term does not need to be computed – saving substantial computational effort. The permeable surface formulation has become a valuable noise prediction tool primarily because CFD has advanced sufficiently to provide the time-dependent flow field solution on the integration surface with high spatial and temporal fidelity, as required by the permeable surface formulation of the FW–H.

PSU-WOPWOP Capabilities

PSU-WOPWOP is a general purpose Ffowcs Williams–Hawkings (FW-H) solver developed at The Pennsylvania State University by Dr. Brentner and his research team[15 16 17 18.] The code was originally developed to compute the noise of rotorcraft in maneuvering flight, but was developed using an object-oriented design in the Fortran 95 language in a very general manner. Both the classical and permeable surface formulations of the FW-H equation[19], as expressed by Farassat's

Formulation 1A[20 21], have been implemented in the code and have been thoroughly tested.

The PSU-WOPWOP code has extensive source motion capability—originating from its roots as a maneuver noise prediction tool. The integration surfaces (solid or permeable) may be either rigid or flexible. PSU-WOPWOP predicts the acoustic pressure time history in the near and far fields, for either stationary or arbitrarily moving observers. PSU-WOPWOP also has significant output signal processing to convert the acoustic pressure time history into acoustic spectra, including narrow band spectra, 1/nth octave bands, etc. The code's output processing also includes the ability to filter the data over arbitrary frequency ranges and include various types of windowing functions for the frequency domain processing.

PSU-WOPWOP has recently been upgraded to predict the acoustic pressure gradient at arbitrary observer locations[22 23.] The acoustic pressure gradient is an input to either frequency or time domain acoustic scattering codes, which then can predict the scattered field when rigid bodies are in the vicinity of the noise predicted by PSU-

© 2018 Tecplot, Inc. All rights reserved worldwide. Tecplot®, Tecplot 360™ and the Tecplot 360™ Logo are registered trademarks and "Master the View™" is a trademark of Tecplot, Inc., Bellevue, WA, USA. All other trademarks are the property of their respective owners.

WOPWOP. PSU-WOPWOP has been used for rotor noise prediction, landing gear noise prediction, acoustic scattering, prediction of trailing edge noise, and jet noise.

In the current work, the permeable integration surfaces (also referred to as acoustic data surfaces or ADS) will be used for the FW-H noise prediction. PSU-WOPWOP will require the time-dependent location of the surfaces along with the time dependent specification of density, momentum and pressure at each of the surface mesh points.

The computation of the acoustic pressure at a large number of observer positions, as might be used, for example, in an extensive phased array, should be very efficient because PSU- WOPWOP uses an observer parallel implementation, employed via the Message Passing Interfaces (MPI). This parallelism effectively sends the acoustic computation for each observer to single processor on a computer cluster, up to the number of processors available. As the processors become free, a new observer position is sent to the processor, keeping all the processors busy until the entire job is done. PSU-WOPWOP has previously been coupled with OVERFLOW and several other CFD codes using a file-based method, which is relatively easy to implement and should be ideal for this project.

Data Transfer Between OVERFLOW and PSU-WOPWOP

In order to use PSU-WOPWOP to predict the acoustic farfield, it is necessary to translate the information about the wind turbine near-field predicted by OVERFLOW into a form that PSU- WOPWOP can work with.

The option chosen for the current work is to use OVERFLOW's capability to save solution data in specified regions of the flow (the "SPLITM" controls). By selecting an appropriate set of surfaces, a reasonable integration surface can be assembled around the spinning blade. The SPLITM data can then be assembled into the "patch file" (containing the surface mesh data at each time step) and "flow data file" (containing the density, momentum, and pressure on the surface at each time step) needed by PSUWOPWOP.

There are two drawbacks to the SPLITM approach. One is that OVERFLOW saves a separate file for each SPLITM surface specified. Also, a new file is created every time the SPLITM data is output to the disk. Since each SPLITM surface must come from only one block, multiple surfaces (twelve, in fact) are required in order to construct the FW-H surface. As a result, the original planned run of 14,400 time steps would have resulted in over 150K files which would have to be processed. Even though this planned run was not completed, there were still over 80K SPLITM files which required processing.

A new utility was written to semi-automatically assemble all of these SPLITM files into the patch and flow data files which PSU-WOPWOP reads.

Beamform Interactive Beamforming Analysis Software

Beamform Interactive is a commercial product of OptiNav, Inc. for processing microphone array data. There are several different modules in Beamform Interactive, which allow the user to apply various beamforming methods to analyze the data. The most basic method is the "Conventional Beamforming" algorithm. This is a high speed, wide band implementation of the classical formula. An "Enhanced Resolution" variant of the classical beamforming technique is also available. This approach weights cross spectral matrix elements to improve resolution. Another algorithm available is DAMAS2. This is a high-speed version of DAMAS which employs an FFT for improved processing speed. It also used a nonuniform mesh to avoid problems with the PSF model. The CLEAN-SC method is an implementation of Sijitsma's algorithm24, which is another deconvolution-based approach to beamforming. Finally, TIDY is an OptiNav method, related to CLEAN-SC, which allows analysis with unlimited bandwidth.

Data transfer between PSU-WOPWOP and Beamform Interactive

PSU-WOPWOP outputs its results in a variety of files and file formats. Of particular interest for the current work was the acoustic pressure history at each microphone location of the virtual phased array. PSU-WOPWOP creates a text file compatible with Tecplot which contains pressure data, including thickness acoustic pressure, loading acoustic pressure, and total acoustic pressure. Tecplot 360 was used to read in this data for each microphone location and extract a history of the total acoustic pressure as a function of time to a separate file. These files were then stitched together into a single file was sent to Dr. Dougherty to be used for the beamforming analysis.

© 2018 Tecplot, Inc. All rights reserved worldwide. Tecplot®, Tecplot 360™ and the Tecplot 360™ Logo are registered trademarks and "Master the View™" is a trademark of Tecplot, Inc., Bellevue, WA, USA. All other trademarks are the property of their respective owners.

Numerical Studies of Wind Turbine Acoustics

Problem Identification

The configuration used for the current work is based on the U.S. Department of Energy National Renewable Energy Laboratory (NREL) 10m diameter research wind turbine, shown in Figure 1. This device has been field tested field-tested in various configurations since 1989 at DOE's National Wind Technology Center located near Boulder, Colorado.

The device has also been tested in NASA's 24.4 by 36.6 meter (80' by 120') wind tunnel. This tunnel is part of the National Full-Scale Aerodynamics Complex (NFAC) which is located at the NASA Ames Research Center in Moffett Field.

The specific case modeled here was based on the "H-sequence" tunnel runs, with a 10 m/s freestream velocity, no yaw, and the blades at 3 degree pitch. The turbine geometry was assumed to be rigid, and the effects of tunnel walls and unsteady inflow conditions were ignored. Also, the "cone" shown upstream of the rotor in Figure 1 was not present in either the wind tunnel experiment being replicated or in the simulation.

Figure 1: The NREL 10m research wind turbine

Computational Mesh

A near-body computational mesh for the NREL wind turbine geometry was obtained from Drs. Chris Stone and Marilyn Smith, who developed the mesh under contract from the National Science Foundation. This mesh consisted of 2.6 million points in 16 blocks. As mentioned above, Cartesian off-body meshes were automatically generated to fill in the remainder of the flow domain. The basic layout of the geometry is shown in Figure 2.

A close-up of the surface mesh in the rotor tip region is shown in Figure 3. The mesh is clustered toward the leading edge, trailing edge, and the tip, but away from these regions, the spanwise spacing of points becomes fairly large, considering the nature of the acoustics we wish to resolve. If more computational resources were available, this is one aspect of the mesh which would have been modified in order to better resolve the unsteady shedding. The present mesh does capture significant unsteadiness, however, as will be shown below.

Figure 2: Modeled NREL 10 m wind turbine geometry (solid surfaces)

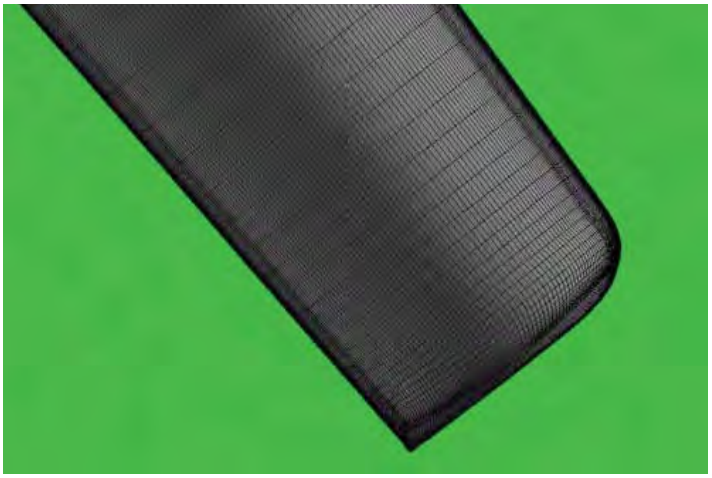

Figure 3: Surface computational mesh in the blade tip region of the NREL 10 m research wind turbine

Figure 4 shows a similar plot to Figure 3, but for the surface mesh near the rotor hub. Again, the spanwise spacing of points is somewhat coarse, but the surface mesh does have good resolution along the chord and also normal to the surface (not shown). above, Cartesian

© 2018 Tecplot, Inc. All rights reserved worldwide. Tecplot®, Tecplot 360™ and the Tecplot 360™ Logo are registered trademarks and "Master the View™" is a trademark of Tecplot, Inc., Bellevue, WA, USA. All other trademarks are the property of their respective owners.

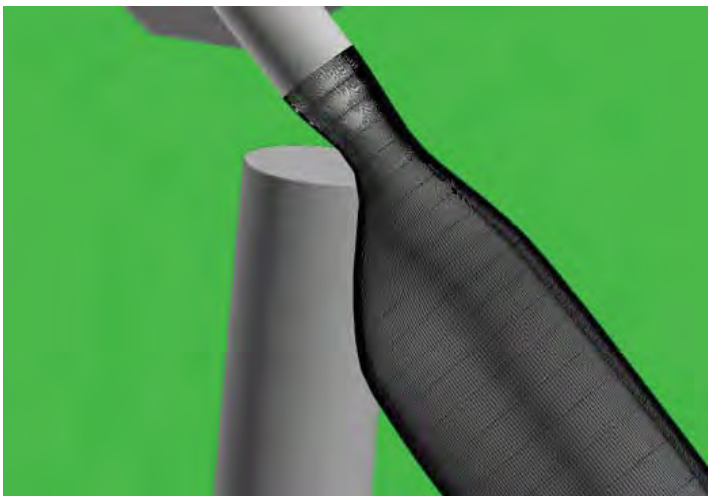

Figure 4: Surface computational mesh in the blade near-hub region of the NREL 10 m research wind turbine

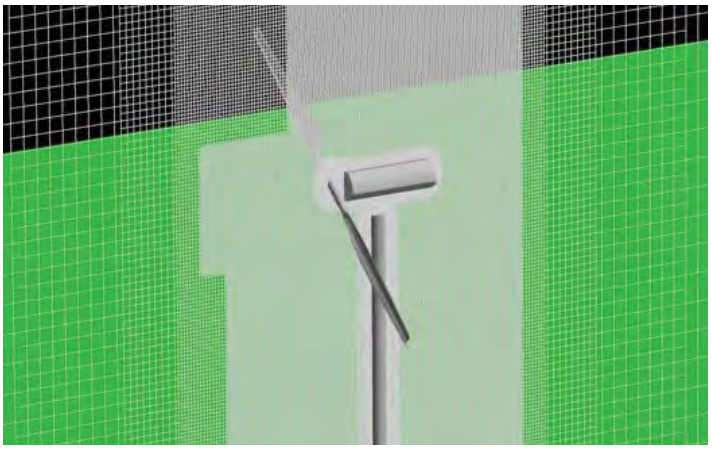

Figure 5: Cross-section through the centerline of the mesh near the start of the simulation (after 8 time steps)

A cross-section of the computational mesh through the centerline of the turbine is shown in Figure 5. In this view, the automatically generated off-body Cartesian meshes are readily seen. As the flow has only advanced for eight time steps at this point (one degree of blade rotation), the automatic mesh refinement algorithm has not modified the initial Cartesian meshes. The need for the automatic mesh refinement is clearly seen in Figure 5, where, beyond about three meters aft of the nacelle, the mesh becomes too coarse to resolve any significant unsteadiness.

Results

CFD Results

A mentioned above, the case modeled here had a constant inflow velocity of 10 meters per second, and the wind turbine was perfectly aligned with the freestream. The reference Mach number, based on tip speed, was 0.11158. The time required for a complete rotation of the blades was approximately 0.83 seconds. The Reynolds number was 2.67 million.

The flowfield solution was been advanced for a total of 7152 time steps (over multiple runs), with a solution saved every 16 steps. For the fixed time step which was used, this corresponds to solutions saved at every two degrees of rotation, and a total rotation for the blades of 894 degrees. The following plots were made using a solution at step 5,696.

Note that, because of the automatic mesh refinement, the original 30.5 million point mesh (in 68 blocks) grew to have more than 5600 blocks with more than 260 million points. Further, had the simulation continued, the point count would have increased still more, because the unsteady flowfield still had not propagated to the edges of the domain.

Figure 6 shows a portion of a centerline cross-section of the mesh at a representative time (corresponding to step 5696). For clarity, the plot shows only every other point in each direction. The region where the adaptive mesh refinement has been active is clearly visible and corresponds closely to the extent that the solver has propagated the vortical structures shed from the turbine.

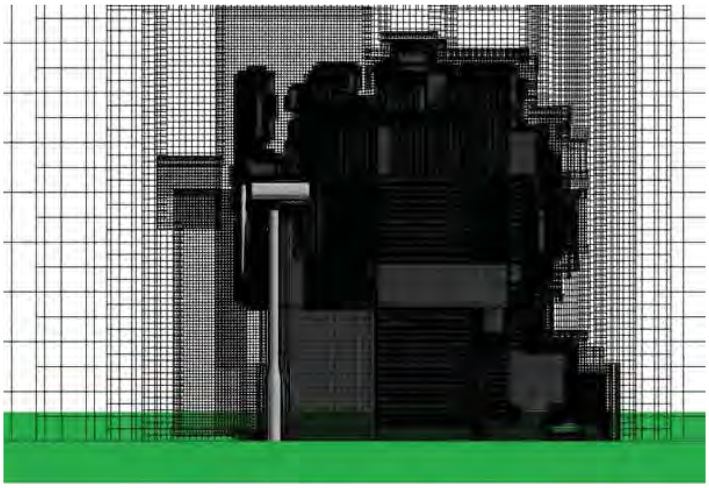

Figure 6: Mesh cross-section along centerline after 5696 steps (every other point plotted)

© 2018 Tecplot, Inc. All rights reserved worldwide. Tecplot®, Tecplot 360™ and the Tecplot 360™ Logo are registered trademarks and "Master the View™" is a trademark of Tecplot, Inc., Bellevue, WA, USA. All other trademarks are the property of their respective owners.

Figure 7 shows the surface pressure on the wind turbine, the ground plane, and a translucent plane at y = -7m (seven meters below the center of the rotor). The traces of vortex shedding can be seen clearly on the translucent plane, and faint traces of something similar can be seen on the ground plane downstream of the mast.

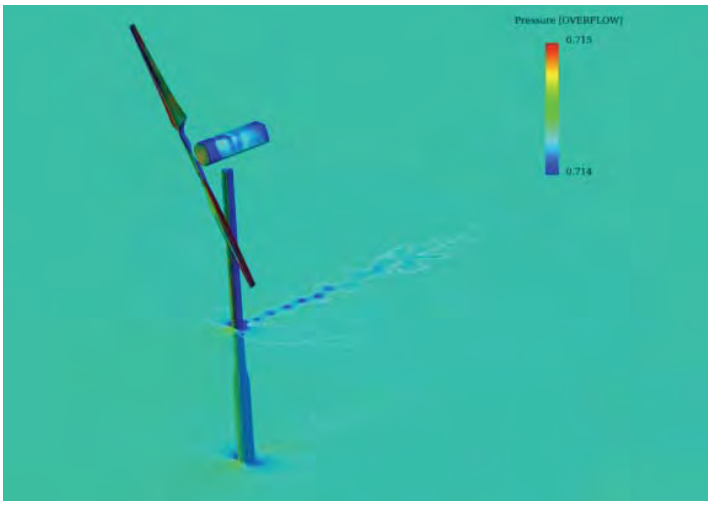

Figure 7: Computed surface pressures on the 10 meter wind turbine

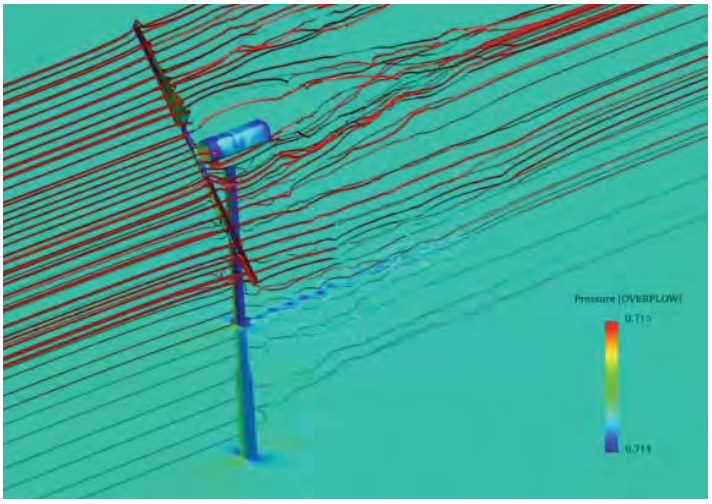

Figure 8: Streamlines of flow around the wind turbine rotor

Figure 9 shows an iso-surface of vorticity magnitude. Here, the tip vortices shed as the rotor spins are clearly visible, as are the vortical structures shed off the mast. Numerous smaller structures are also seen throughout the downstream region.

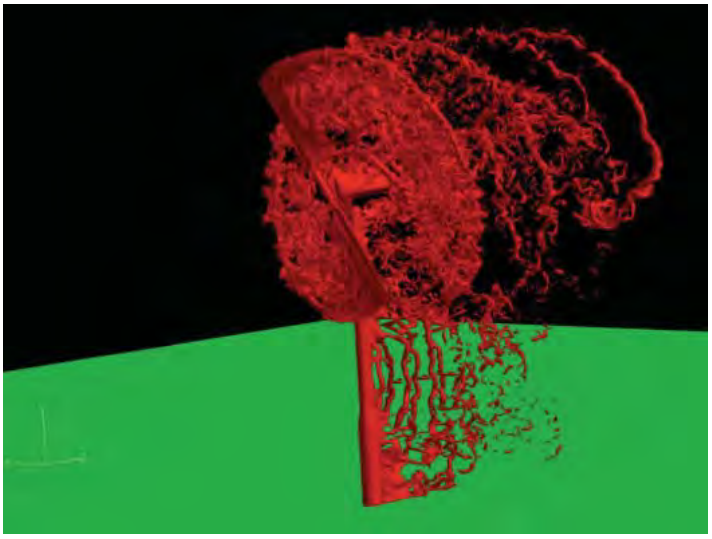

Figure 9: Iso-surface of vorticity magnitude in the flow around the wind turbine

Note that, without automatic mesh refinement, these flow features would not be so well resolved. The initial attempts to run this problem, which did not use AMR, were only able to resolve unsteady features for about half the downstream distance shown here. Further note that this does not represent the limit of OVERFLOW's capabilities, since the vorticity observed here includes the initial transients, which have not yet propagated out of the domain. It thus appears that, to the extent the near-body meshes are able to generate the vortical structures, the off-body Cartesian meshes with AMR are able to propagate them.

An integration of the forces and moments over the entire wind turbine structure, including the mast and nacelle was performed for an earlier run of this case (which ran a total of 5488 with somewhat different AMR settings). The integration technique used was not exact, in that the overlapping meshes used by the OVERFLOW simulation were not precisely accounted for. The results, however, are expected to be proportional to the actual loads, and can thus be used to determine whether or not a time-dependent loading is being predicted.

The coordinate system for this simulation had the oncoming wind blowing in the positive z direction. The y-axis points in the vertical direction, and the x-axis points to the left when facing the front of the turbine. The force (in arbitrary units) in the z-direction is shown in Figure 10 as a function of solution time steps. Recall that the timestep is such that the rotor sweeps out one degree every eight

© 2018 Tecplot, Inc. All rights reserved worldwide. Tecplot®, Tecplot 360™ and the Tecplot 360™ Logo are registered trademarks and "Master the View™" is a trademark of Tecplot, Inc., Bellevue, WA, USA. All other trademarks are the property of their respective owners.

steps. Thus, 2880 steps are required for a full 360 degree sweep. The history plotted in Figure 10 therefore represents only about two full rotations of the rotor. Clearly, the load is trending to some sort of asymptotic value, but it is not clear whether or not any ongoing periodicity will be resolved in this component of the force.

The vertical and side-force components as a function of time are shown in Figure 11 for the same case, along with their combined magnitudes. All of these quantities show a clear unsteadiness, and there are also hints that some sort of periodicity may be setting up. At this point, however, the simulation has not run far enough to detect the presence of harmonics with any certainty.

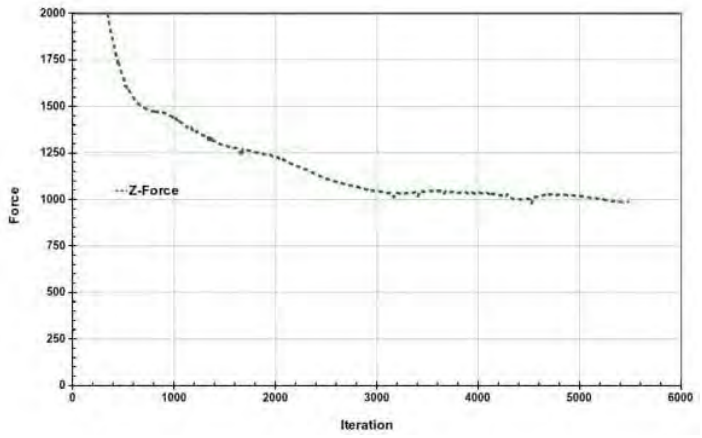

Figure 10: Streamwise force on wind turbine as a function of time step

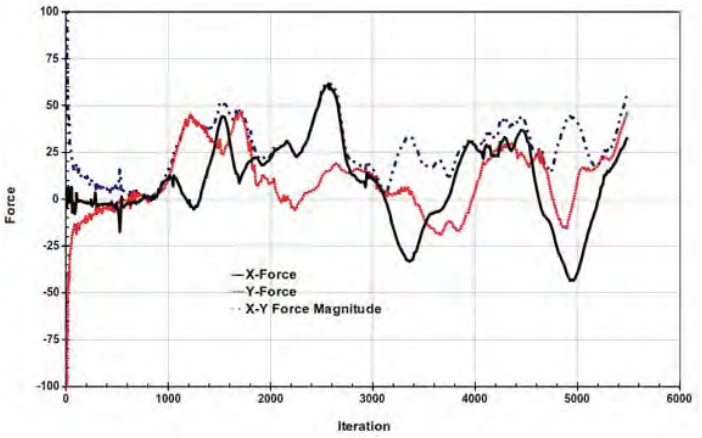

Figure 11: History of forces normal to the streamwise direction on the wind turbine simulation

Another way to look at the unsteadiness in the flow is to examine the vorticity in the wake at various points. The plot of vorticity magnitude in Figure 12 shows that, below the level swept by the rotor, the wake behind the mast takes on a Karmann vortex street structure, which breaks up further downstream.

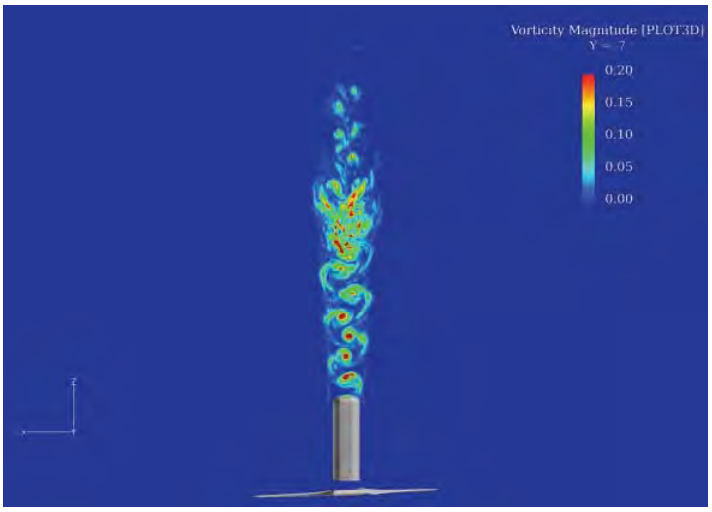

Figure 12: Vorticity magnitude behind the wind turbine mast roughly five meters above the ground plane

Hints of this vortex street can still be seen in the wake higher above the ground plane, such as that shown in Figure 13. In regions behind where the rotor sweeps, the helical structures created by the vortices shed from the blade tips and trailing edges become more dominant. Note the region of strong vorticity which has just been shed from the rotor as one of the blades reached its lowest point the sweep.

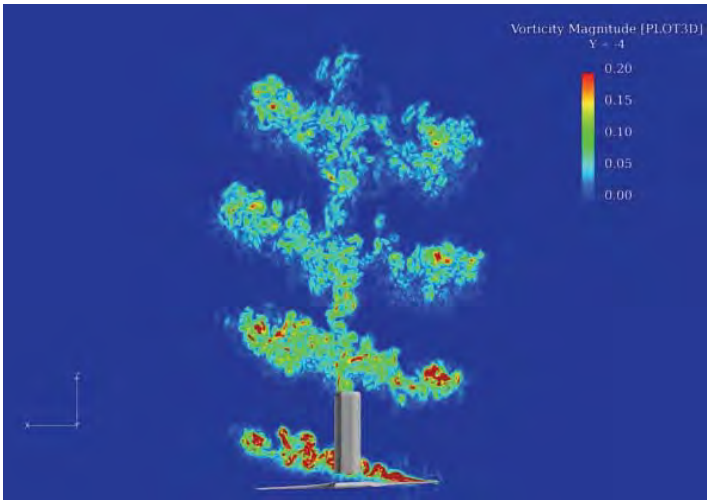

Figure 13: Vorticity magnitude on a constant-y plane one meter above the lower limit of the rotor sweep

© 2018 Tecplot, Inc. All rights reserved worldwide. Tecplot®, Tecplot 360™ and the Tecplot 360™ Logo are registered trademarks and "Master the View™" is a trademark of Tecplot, Inc., Bellevue, WA, USA. All other trademarks are the property of their respective owners.

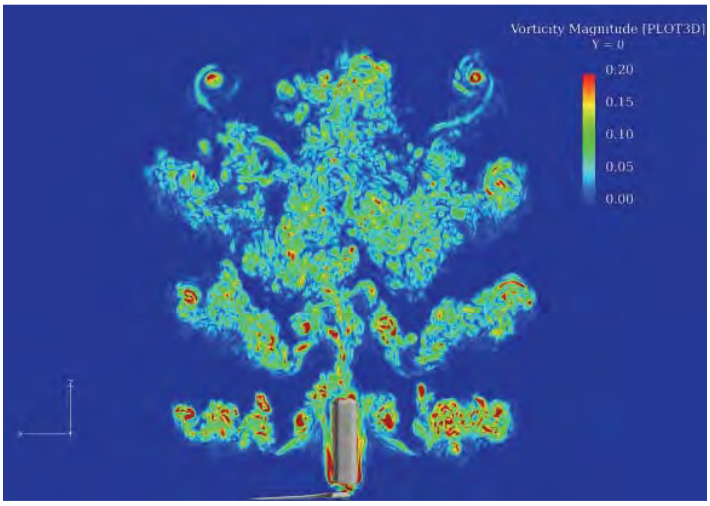

Figure 14: Vorticity magnitude on a constant-y plane through the nacelle centerline

The vorticity magnitude contours shown in Figure 14 are plotted on a horizontal cut through the nacelle centerline (and the rotor hub). The starting vortices are clearly visible at the top of the plot (not having had enough time to propagate beyond the domain. The complex wake vortex interactions are clearly visible.

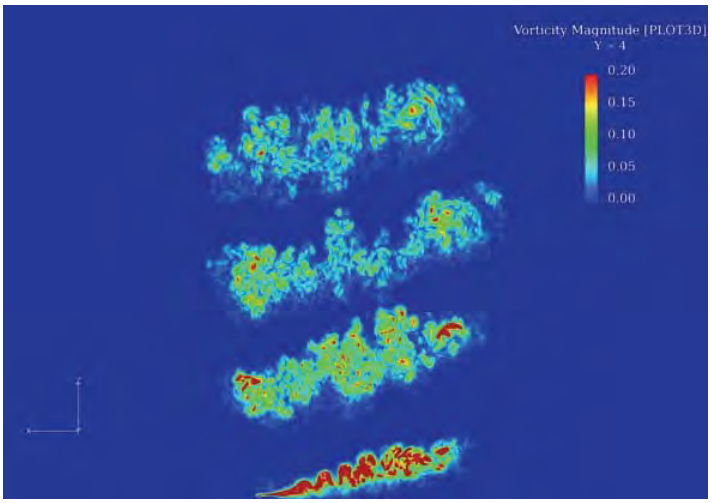

Figure 15: Vorticity magnitude on a constant-y plane one meter below the upper limit of the rotor sweep

The final plane of vorticity magnitude contours is shown in Figure 15. This plane is positioned four meters above the rotor hub (one meter below the maximum height swept by the rotor). This plot is very similar to Figure 13, but lacks the wake from the mast. Again, the simulation predicts a complex interaction of the wake and tip vortices shed from the rotor.

Vortical structures such as those visualized in the preceding Figures are associated with noise emission, but the acoustic field itself consists, of course, of pressure fluctuations. The pressure field is shown in Figure 16 on the same horizontal plane where vorticity magnitude was plotted in Figure 13. The pressure footprints of the vortical structures are clearly evident, but in addition, there are traces of what appear to be acoustical waves radiating away from the turbine and the wake.

Note that, because of the low speed of the flow, the pressure variations in the flow are close to the limits of what can be resolved due to the numerical precision of the calculation. This is a known phenomenon of low speed flows, and is the reason why low Mach number preconditioning was used for these simulations. The fine-grained oscillations observed in the pressure contours are believed to be largely due to the precision limitations, along with the effects of the changing resolution of the overlapping computational meshes, possibly incomplete convergence of the subiteration process, and the lack of dissipation in the fourth order scheme used away from the near-body computational mesh blocks.

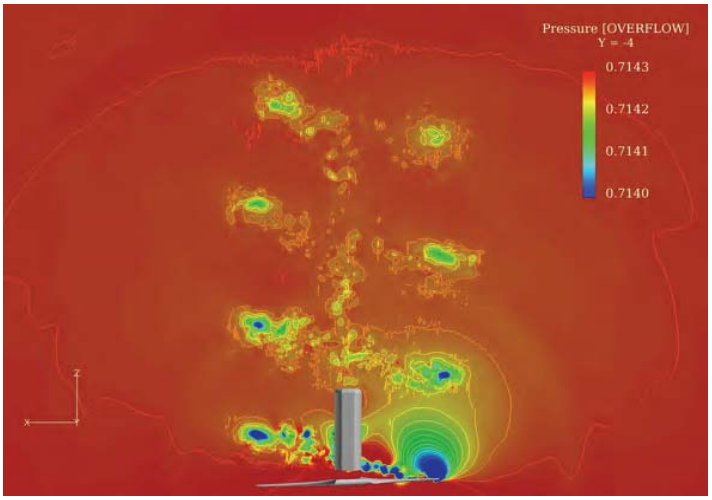

Figure 16: Pressure on a constant-y plane one meter above the lower limit of the rotor sweep

To highlight the acoustical field, the pressure gradient magnitude has been plotted in Figure 17 on the y = -4 plane. This plot clearly shows the radiating pressure waves centered on the rotor. The noise which was present in the pressure field contours is magnified when the gradient is computed. In addition, slight differences in the predicted gradient in overlapping regions results in a noisier appearance to the contours than the flowfield actually warrants.

© 2018 Tecplot, Inc. All rights reserved worldwide. Tecplot®, Tecplot 360™ and the Tecplot 360™ Logo are registered trademarks and "Master the View™" is a trademark of Tecplot, Inc., Bellevue, WA, USA. All other trademarks are the property of their respective owners.

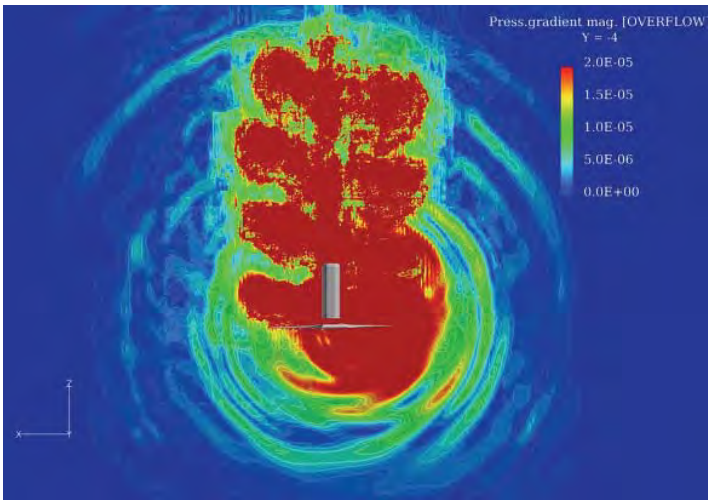

Figure 17: Magnitude of pressure gradient on a constant-y plane

Further, it should be noted, both for the pressure gradient plots and the vorticity magnitude contours, that the gradients used for these quantities are being computed by the flow visualization package using a different algorithm (and boundary conditions) than that used by the OVERFLOW solver for the actual solution. Despite this limitation, the values shown in the plots should be reasonably close to the "actual" values seen by the CFD solver.

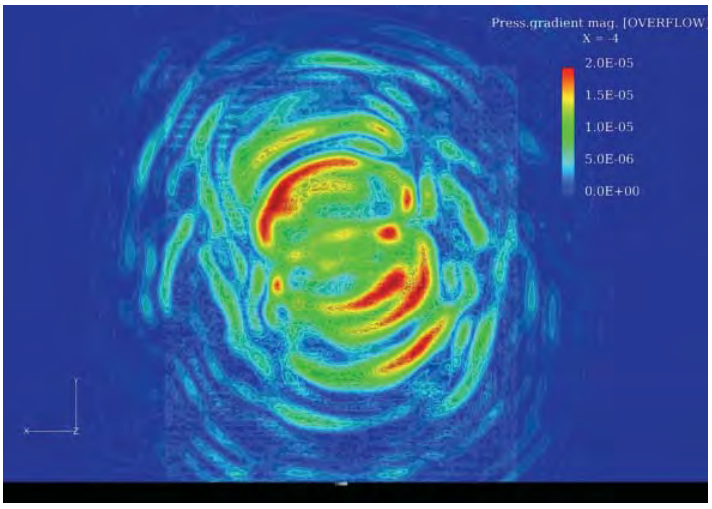

Figure 18: Magnitude of pressure gradient on a constant-x plane upstream of the rotor

A view of the pressure gradient magnitude on a plane upstream of the rotor is shown in Figure 18. Here, the radiating waves are again clearly visible. In addition, there are hints of pressure waves reflecting from the ground plane. The regions of elevated pressure gradient magnitude appear to be related to the rotor position (which is roughly thirty degrees from vertical at this point in the simulation). We believe that these also correspond to regions of increased noise production.

Acoustical Analysis with PSU-WOPWOP

The acoustical analysis of this case was performed by linking the three analysis tools discussed above in Section 2. The first step, as discussed in the previous section, is the prediction of the near-field acoustics using CFD. The middle step of this process is to analyze the CFD results using the PSU-WOPWOP code to predict the total acoustic pressure as a function of time at specific locations in the farfield.

The locations chosen correspond to the microphones of an OptiNav Array 24 phased array. This virtual array was positioned with the center one mast height downstream of the wind turbine and one meter off the ground. The array was rotated to point at the rotor hub, as shown in Figure 19. The array is approximately 0.7 meters across, and the microphone locations have been optimized to provide optimal beamforming results.

Figure 19: Virtual microphone array position

As discussed in Section 2, OVERFLOW's ability to save flow data on specific grid surfaces was employed to collect flow data at every step on acoustic data surfaces surrounding the rotors. Figure 20 shows pressure contours on the acoustic data surfaces at an instant in time.

© 2018 Tecplot, Inc. All rights reserved worldwide. Tecplot®, Tecplot 360™ and the Tecplot 360™ Logo are registered trademarks and "Master the View™" is a trademark of Tecplot, Inc., Bellevue, WA, USA. All other trademarks are the property of their respective owners.

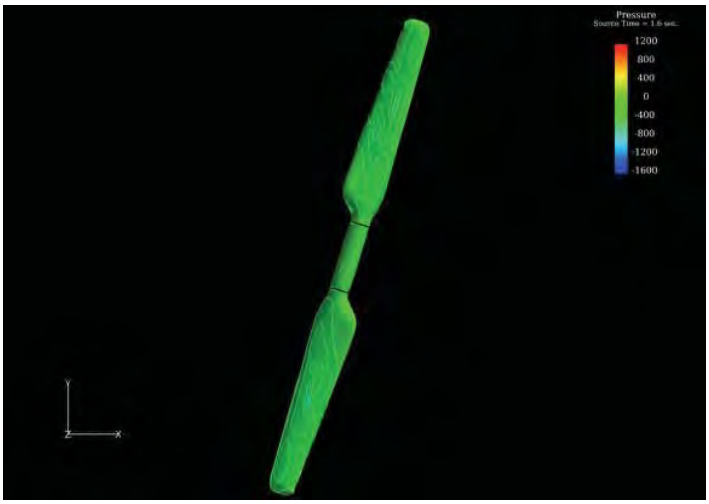

Figure 20: Contours of pressure on the acoustic data surfaces at a representative time

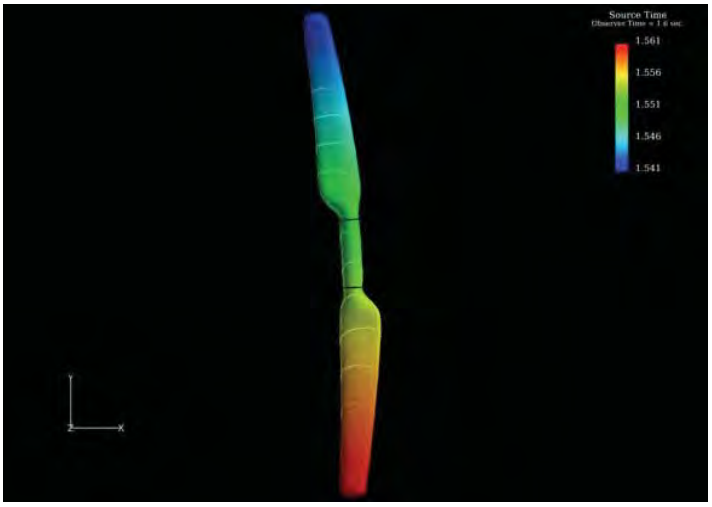

Figure 21: Iso-surface of observer time at the first array microphone location with contours indicating the time of sound emission

Figure 21 shows an iso-surface of "observer time" at the same instant in time. This figure shows how the microphone 1 in the virtual array "sees" the acoustic data surface. The surface is colored by the source time at which the sound being measured passed through the surface. By comparing these values, one can see that the average propagation time was approximately 0.05 seconds, but that this value varies by up to +/- 0.01 seconds when the rotor is vertical. These values agree with the expected behavior, given the mean speed of sound and the position of the microphone. It should be noted that all of the results from PSU-WOPWOP were made without consideration of the ground plane. Though PSU-WOPWOP has the capability to include such a feature in the analysis, we encountered anomalies when we attempted to use it. As we were not able to discover a work-around in time for this paper, the results here are all from analyses without the ground plane feature.

The acoustical analysis was restricted to data taken between t=1.18 and t=2.08 seconds. This range was chosen to avoid initial transients and also some anomalous signals which were observed around the 1.1 second mark. The 0.9 seconds of recorded data which was analyzed corresponds to slightly more than one full rotation of the blades. A trace of the total acoustic pressure, as predicted by PSU-WOPWOP at four different microphone locations, is shown in Figure 22. Obviously, being relatively close together, one does not expect radical differences in the pressures at these locations, and this is what the figure shows. Close inspection reveals that there are some differences in the signal, however, which are more clearly shown in Figure 23. This latter figure zooms in on the last 0.04 seconds and shows how, especially at the first microphone location, the signals do differ from each other in the details.

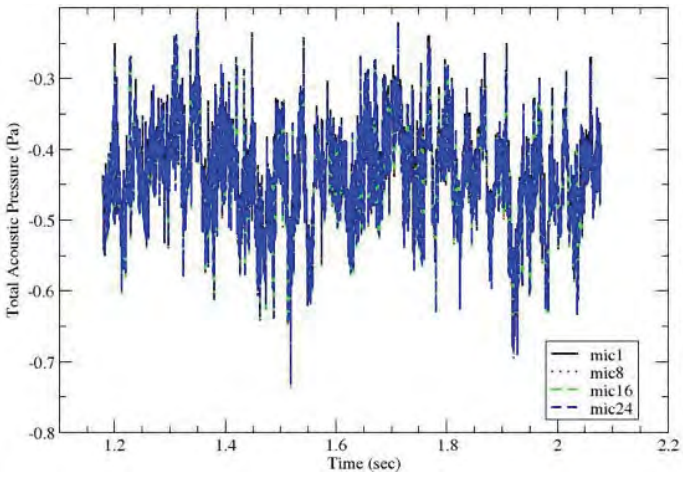

Figure 22: Pressure traces predicted by PSU-WOPWOP at four microphones in the virtual array

© 2018 Tecplot, Inc. All rights reserved worldwide. Tecplot®, Tecplot 360™ and the Tecplot 360™ Logo are registered trademarks and "Master the View™" is a trademark of Tecplot, Inc., Bellevue, WA, USA. All other trademarks are the property of their respective owners.

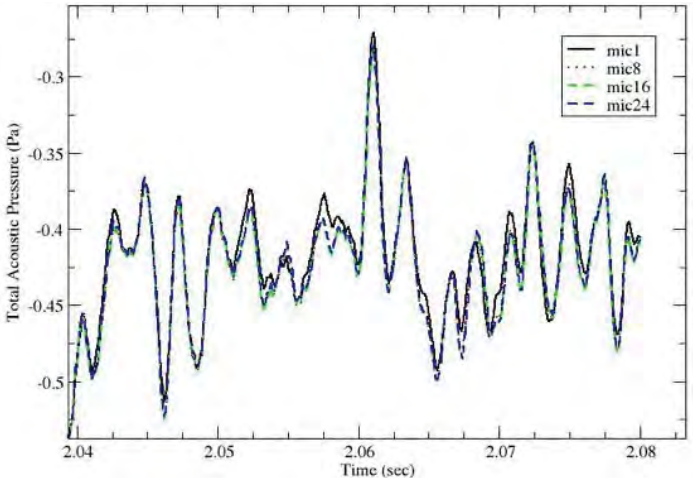

Figure 23: Detailed portion of pressure traces at four locations

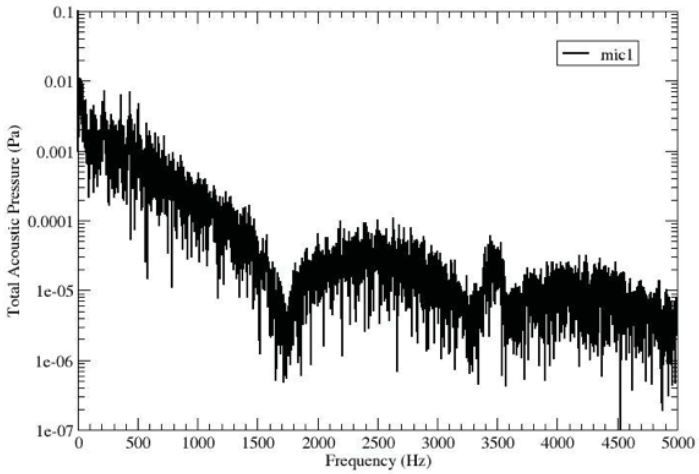

Figure 24: Total acoustic pressure spectrum predicted by PSU-WOPWOP at microphone 1 location

PSU-WOPWOP sampled the predicted acoustic conditions at the Array 24 microphone locations at 9001 evenly spaced times over the 0.9 seconds of interest (a 10kHz sampling rate). Note, however, that the CFD solution only had approximately 3100 steps in that time period at which data was collected on the acoustic data surfaces. The impact of this mismatch can be seen in Figure 24, which shows spectrum of total acoustic pressure predicted at the first microphone of the array. The lower frequencies show a gradual decay of acoustic energy, as expected. Around the Nyquist frequency of the original, however, the predicted noise begins to increase. This is almost certainly an aliasing error in the signal processing.

Looking more closely at the resolvable frequencies below 1500 Hz, Figure 25 shows a sequence of significant peaks in the spectrum. However, there is no obvious fundamental frequency of which all the other peaks are multiples.

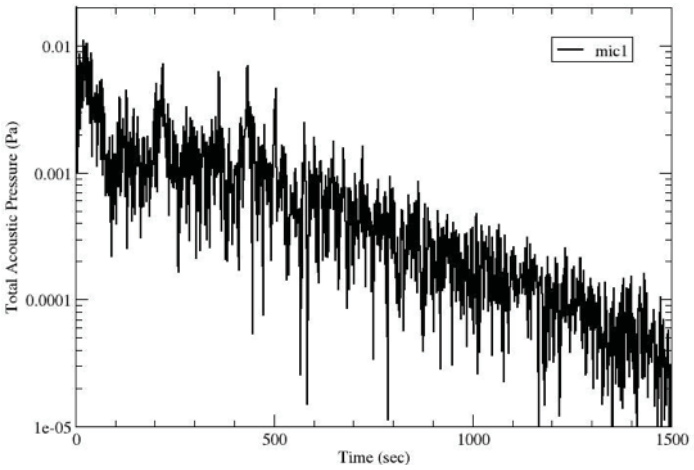

Figure 25: Lower frequency region of the total acoustic pressure spectrum predicted by PSU-WOPWOP at microphone 1 location

PSU-WOPWOP predicted the overall sound pressure level at the virtual microphone array locations as all being in the vicinity of 85 db, as shown in Figure 26

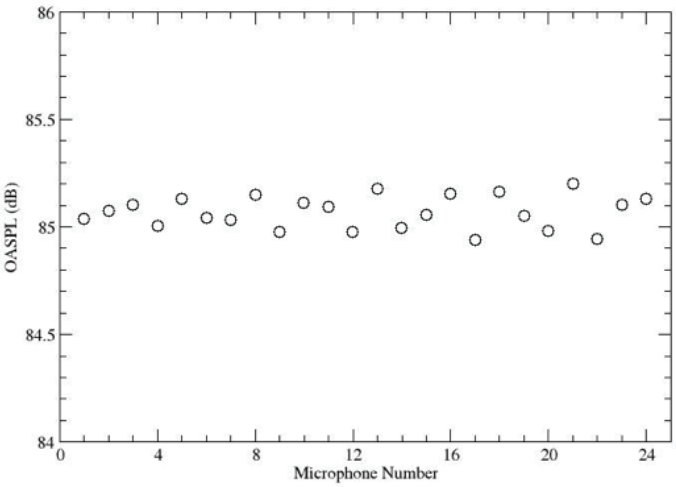

Figure 26: Predicted OASPL at microphone locations in virtual array

© 2018 Tecplot, Inc. All rights reserved worldwide. Tecplot®, Tecplot 360™ and the Tecplot 360™ Logo are registered trademarks and "Master the View™" is a trademark of Tecplot, Inc., Bellevue, WA, USA. All other trademarks are the property of their respective owners.

Beamforming of Virtual Microphone Array Data

The pressure traces at the virtual array locations were analyzed using the Beamform Interactive software.

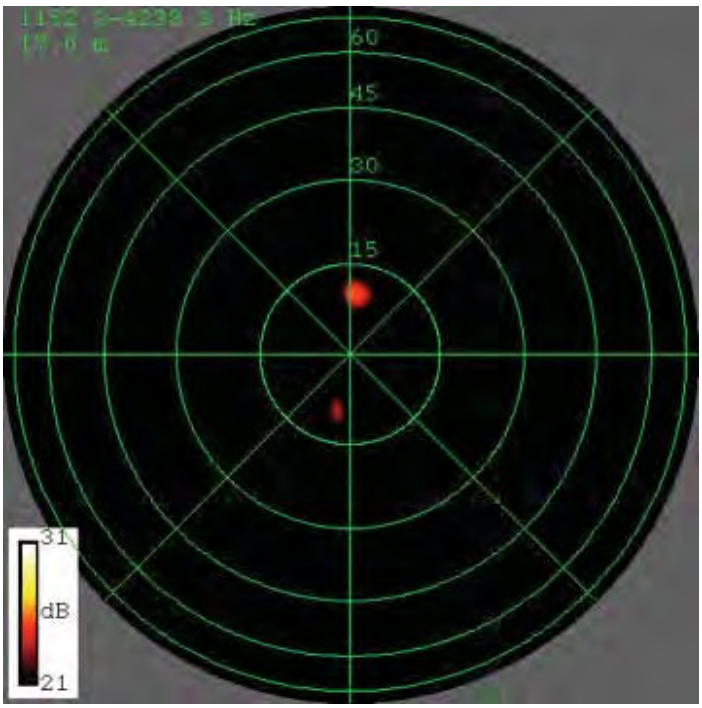

Figure a) Rotor approximately vertical

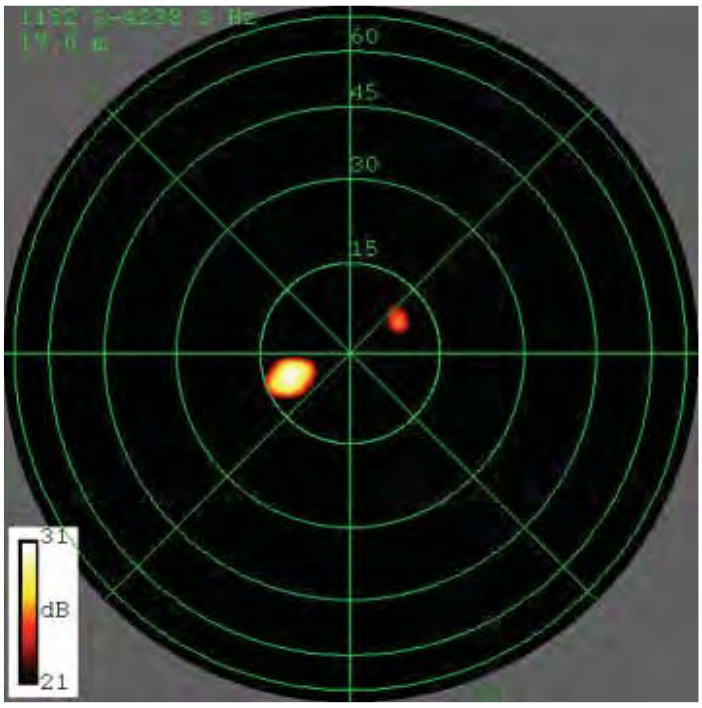

Figure b) Rotor at ~45 deg.

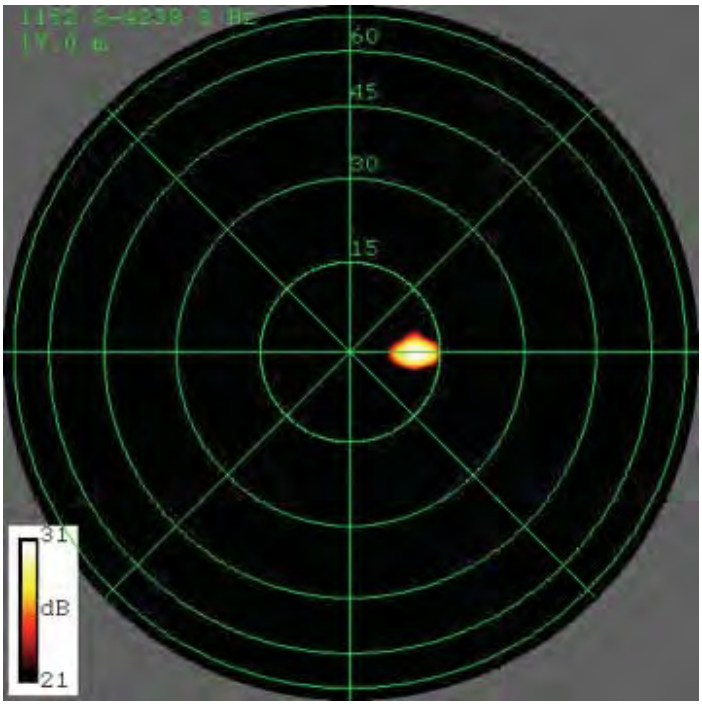

Figure c) Rotor at ~90 deg.

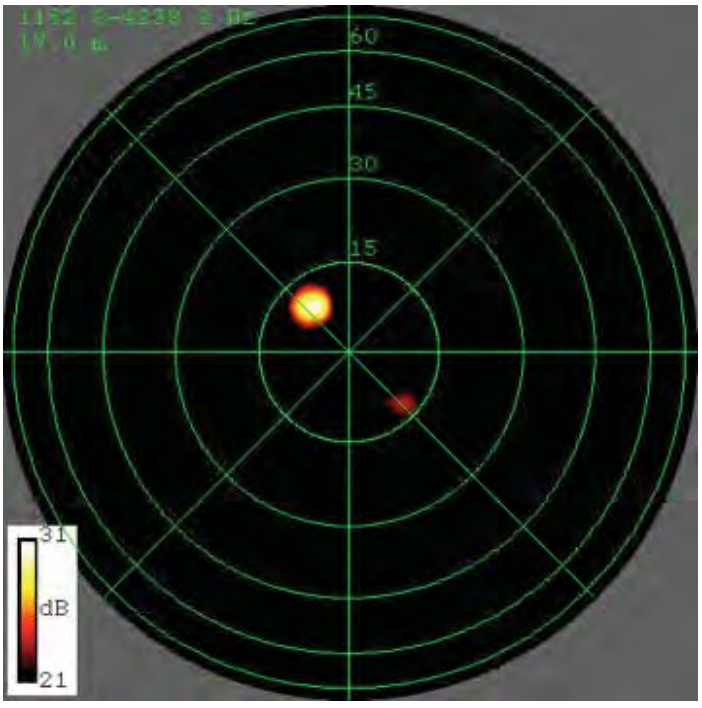

Figure d) Rotor at ~135 deg.

Figure 27: Sound sources identified by beamforming the virtual microphone array signals over the first half of one rotation of the turbine rotor

© 2018 Tecplot, Inc. All rights reserved worldwide. Tecplot®, Tecplot 360™ and the Tecplot 360™ Logo are registered trademarks and "Master the View™" is a trademark of Tecplot, Inc., Bellevue, WA, USA. All other trademarks are the property of their respective owners.

Selected frames from the resulting video are shown in Figures 27 and 28. The first frame (27a) shows predicted noise sources when the rotor is oriented nearly vertically. The remaining frames are taken roughly every 45 degrees of blade rotation. It is more easily seen in the animation than these stills, but there are a number of features being resolved that appear correct. These include the tip source location (it is at about the right polar angle) and the preference for the advancing blade.

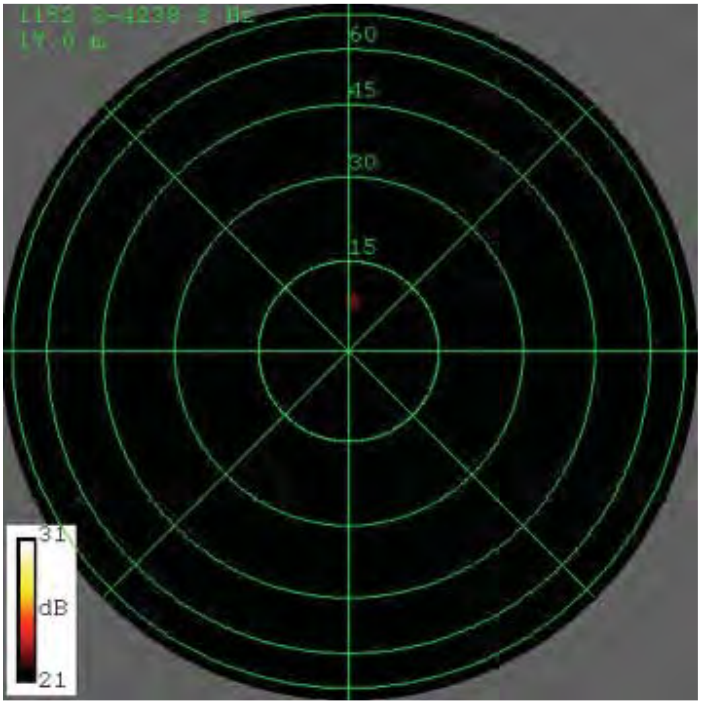

Figure a) Rotor at ~180 deg.

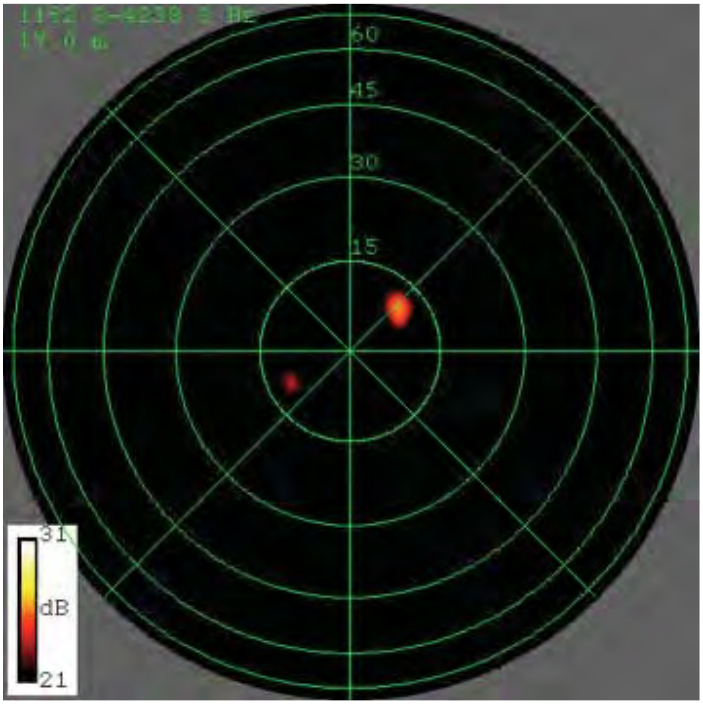

Figure b) Rotor at ~225 deg.

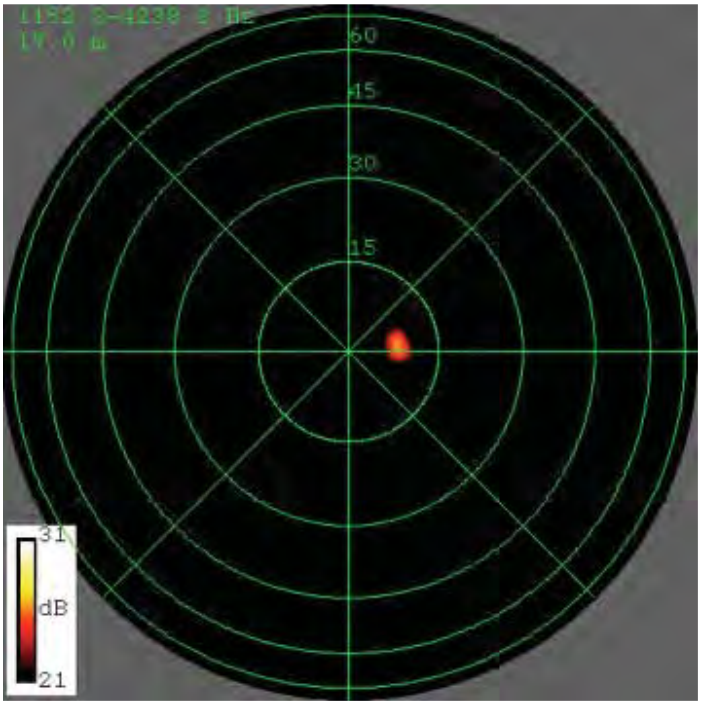

Figure c) Rotor at ~270 deg.

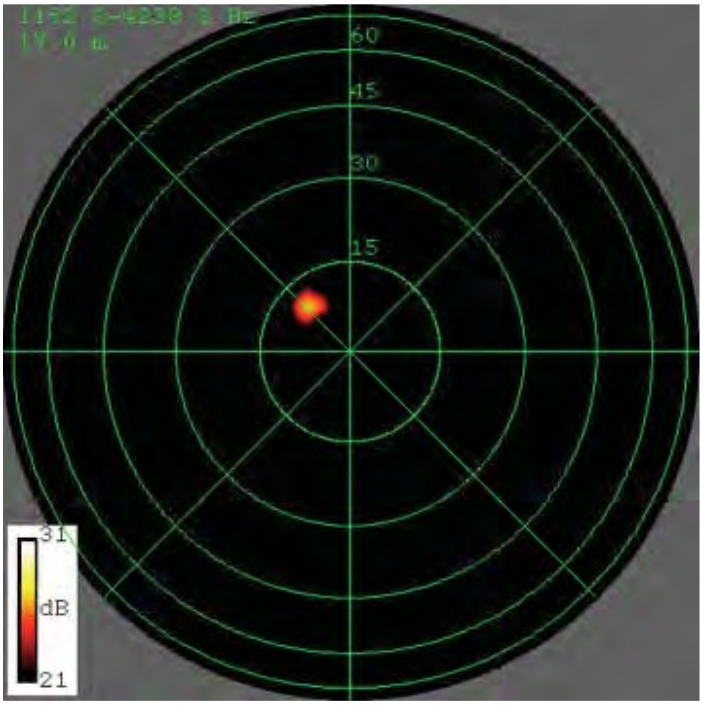

Figure d) Rotor at ~315 deg.

Figure 28: Sound sources identified by beamforming the virtual microphone array signals over the second half of one rotation of the turbine rotor

© 2018 Tecplot, Inc. All rights reserved worldwide. Tecplot®, Tecplot 360™ and the Tecplot 360™ Logo are registered trademarks and "Master the View™" is a trademark of Tecplot, Inc., Bellevue, WA, USA. All other trademarks are the property of their respective owners.

It was found that the following settings obtained the best results:

- Subtract the array average from each time point
- Use the TIDY algorithms
- Use the "enhanced resolution" option
- Select a somewhat high frequency band

The approach taken here to subtract the average was used because there was a huge source in the center of the image that we could not get rid of any other way. A disadvantage of this approach is that is steers a null to the center of the picture, so the results end up being bad for frequencies that are not high enough for the array to resolve the center from the tip region. For this reason, it was necessary to bias to high frequency. This could be helped by repeating the analysis with a larger array.

We believe that the need for this subtraction of the array average stems from the nominal CFD average pressure changing over time. Figure 29 shows a running average of the total acoustic pressure at the various microphone locations. The average was taken over 1000 time steps at a time (out of the 9001 steps covering 0.9 seconds of simulated time output by PSU-WOPWOP). It is clear that the average value is not zero, indicating that the CFD-predicted pressure at the microphone array was not identical to the nominal atmospheric pressure. Also, the running average varies noticeably over time. In fact, it may be that a better strategy for processing synthetic array data such as this would be to subtract out the running average, rather than a single overall average over all time.

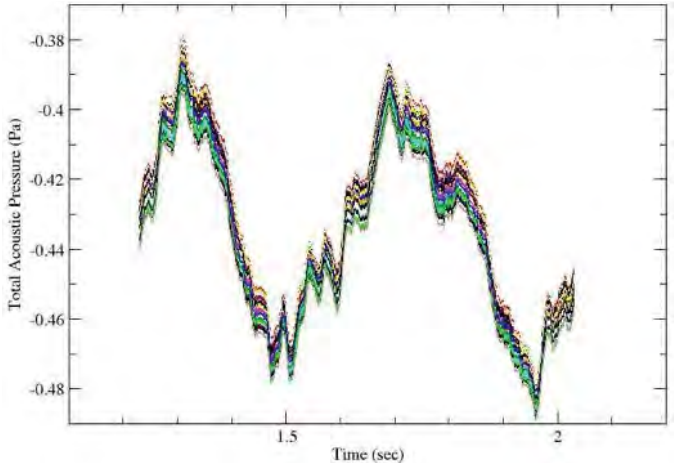

Figure 29: Running average of total acoustic pressure predicted at the virtual array microphone locations

Conclusions

All of the pieces have been assembled to enable a full acoustic analysis using numerical simulations of the flow around an operational wind turbine. The OVERFLOW code solves the unsteady Navier-Stokes equations to predict the acoustic near-field. The near-field data is used by the PSU-WOPWOP Ffowcs-Williams Hawkings solver to propagate the acoustic field to the farfield. Farfield data is then recorded at locations corresponding to a microphone array, and this data is processed using the Beamform Interactive analysis software.

Demonstrations of each of these pieces were presented above, and the process is able to predict the expected broadband noise sources focused near the rotor tips. This is despite several obstacles which had to be worked around in the course of the project.

Several of the identified shortcomings of the current results involve the limitations of the CFD solution. For example, limited computational resources, required that we permit only a single level of automatic mesh refinement for the current work. With increased computational resources, another level of refinement might be possible, which would greatly enhance the ability of the solver to propagate the unsteady vortical flow in the rotor wakes. It is likely that such refinement would result in computational meshes with billions of points, however, so the resource requirements would be significant.

In addition, a programming error in OVERFLOW (now fixed) prevented our solutions from continuing if restarted from a previous solution. Thus, whenever a simulation stopped for any reason (e.g. a hardware problem on one of the nodes), it was necessary to re-run the entire simulation from scratch. As a result, the originally planned 14,400 time steps were never completed. Having a longer time series to work with would, no doubt, improve the quality of the results. It would, for example, allow the initial transients to propagate further downstream prior to sampling the data.

More available computer resources would also allow the resolution of the near-body computational meshes to be improved, with a corresponding improvement to the predicted acoustic near-field. Due to the nature of the synthetic array technique, an improved CFD solution leads directly to an improved prediction of farfield noise and noise source location.

© 2018 Tecplot, Inc. All rights reserved worldwide. Tecplot®, Tecplot 360™ and the Tecplot 360™ Logo are registered trademarks and "Master the View™" is a trademark of Tecplot, Inc., Bellevue, WA, USA. All other trademarks are the property of their respective owners.

Several other issues arose in the course of the PSU-WOPWOP analysis. First, though the use of the SPLITM surface saving capability in OVERFLOW was convenient, in retrospect, it is probably advisable to embed custom acoustic data surfaces in the computational mesh and record the data on them. This would ensure that no issues arise due to any discontinuity in the surfaces (which happens because they are currently made up of surfaces chosen from non-point-matched overlapping meshes). It might also be possible, by designing the surfaces appropriately, to decrease the number of points at which data is saved, with a consequent decrease in file size and data processing time.

In addition, we were unable to make use of PSU-WOPWOP's ability to predict the effect of the ground plane on the acoustics. Thus, we do not clearly see the expected enhanced noise emitted by the downward sweeping blade relative to the upward sweeping one. We continue to investigate the source of this problem.

Challenges were noted in the beamforming process. As discussed above, these may be due to a non-zero (and varying) average total acoustic pressure predicted at the virtual array. Combining the ideas presented in the previous discussion for possible improved techniques for dealing with such condition, with a longer time sequence of data to work with, we believe that improved beamforming results could be obtained.

Despite the aforementioned limitations to the analysis presented here, we feel that the overall technique has been successfully demonstrated. The synthetic array technology was shown to be able to identify the locations of the major noise sources of the NREL wind turbine, and the limitations identified above could all be addressed by available technology. We feel, therefore, that this technology is viable and offers a realistic possibility of screening wind turbine designs for acoustical qualities prior to building and operational testing.

Tecplot 360. Tecplot 360's suite of visualization & analysis tools integrates CFD post-processing, field and parametric data management, and powerful analytics into a single environment. An engineer using Tecplot 360 can manage and analyze collections of CFD simulations, and compare them in a single environment while evaluating overall system performance.

Learn about using Tecplot 360 for parametric CFD analysis:

https://www.tecplot.com/360

Acknowledgements

The authors wish to acknowledge Drs. Chris Stone and Marylin Smith for providing the near- body computational mesh used for this work, which they created under NSF funding. Further, Dr. Stone provided valuable advice for setting up and running the OVERFLOW solver. Dr. Chris Hannes assisted in developing the strategy used with OVERFLOW for accumulating the data to be transferred to PSU-WOPWOP.

This work was sponsored by the United States Department of Energy under DoE award DE- EE0002979.

References

1 Kandula, M. and Buning, P. G., 1994, "Implementation of LU-SGS Algorithm and Roe Upwinding Scheme in OVERFLOW Thin-Layer Navier-Stokes Code," AIAA Paper 1994- 2357.

2 Jesperson, D., Pulliam, T., and Buning, P., 1997, "Recent enhancements to OVERFLOW," AIAA Paper 1997-0644.

3 Vassberg, J. C., Buning, P. G., and Rumsey, C. L., 2002, "Drag prediction for the DLR-F4 wing/body using OVERFLOW and CFL3D on an overset mesh," AIAA Paper 2002-0840.

4 Bounajem, E., 2001, "Prediction of business jet airloads using the OVERFLOW Navier- Stokes code," AIAA Paper 2001-1004.

5 Olsen, M. E. and Prabhu, D. K., 2001, "Application of OVERFLOW to hypersonic perfect gas flowfields," AIAA Paper 2001-2664.

© 2018 Tecplot, Inc. All rights reserved worldwide. Tecplot®, Tecplot 360™ and the Tecplot 360™ Logo are registered trademarks and "Master the View™" is a trademark of Tecplot, Inc., Bellevue, WA, USA. All other trademarks are the property of their respective owners.

6 Buning, P. G., Gomez, R. J., and Scallion, W. I., 2004, "CFD Approaches for Separation of Wing-Body Stage Separation," AIAA Paper 2004-4838.

7 Nichols, R., Tramel, R., and Buning, P., 2006, "Solver and Turbulence Model Upgrades to OVERFLOW 2 for Unsteady and High-Speed Applications," AIAA Paper 2006-2824.

8 Nichols, R., Tramel, R., and Buning, P., 2007, "Evaluation of Two High Order WENO Schemes," AIAA Paper 2007-3920.

9 Lighthill, M. J., 1952, "On Sound Generated Aerodynamically: I. General Theory," Proc. Roy. Soc. Lond. A, Vol. 211, 564-587.

10 Lilley, G. M., 1974, "On the Noise from Jets," Noise Mechanisms, AGARD-CP-131, 13.1- 13.12.

11 Khavaran, A., Krejsa, E. A. and Kim, C. M., 1994, "Computation of Supersonic Jet Mixing Noise for an Axisymmetric Convergent Divergent Nozzle," J. of Aircraft, Vol. 31, No. 3, 603-609.

12 Khavaran, A., 1999, "Role of Anisotropy in Turbulent Mixing Noise," AIAA Journal, 37(7), 832-841.

13 Ffowcs Williams, J. E., and Hawkings, D. L., 1969, "Sound Generated by Turbulence and Surfaces in Arbitrary Motion," Philosophical Transactions of the Royal Society, Vol. A264, No. 1151, 321–342.

14 Brentner K.S., and Farassat F., 1998, "An analytical comparison of the acoustic analogy and Kirchhoff formulation for moving surfaces," AIAA J, Vol. 36, No. 8, 1379–1386.

15 Brès, G. A., 2002, "Modeling the noise of arbitrary maneuvering rotorcraft: Analysis and implementation of the PSU-WOPWOP noise prediction code," M.S. thesis, Department of Aerospace Engineering, The Pennsylvania State University.

16 Perez, G., 2002, "Investigation of the influence of maneuver on rotorcraft noise," M.S. thesis, Department of Aerospace Engineering, The Pennsylvania State University.

17 Brentner, K. S., Perez, G., Brès, G. A., and Jones, H. E., 2003, "Maneuvering Rotorcraft Noise Prediction," Journal of Sound and Vibration, Vol. 39 (3-5), 719–738.

18 Hennes, C., Lopes, L., and Shirey, J., 2009, PSUWOPWOP User's Manual, The Pennsylvania State University, University Park, PA.

19 Brentner, Kenneth S, and Farassat F., 2003, "Modeling Aerodynamically Generated Sound of Helicopter Rotors," Progress in Aerospace Sciences, Vol. 39, No.2–3, 83–120.

20 Farassat, F., and Succi, G. P., 1983, "The Prediction of Helicopter Discrete Frequency Noise," Vertica, Vol. 7 (4), 309–320.

21 Farassat, F., 2007, "Derivation of Formulations 1 and 1A of Farassat," NASA TM 2007- 214853.

22 Lee, S., Brentner, K. S., Farassat, F., and Morris, P. J., 2009, "Analytic Formulation and Numerical Implementation of an Acoustic Pressure Gradient Prediction," Journal of Sound and Vibration, Vol. 319 (3–5), 1200–1221.

23 Lee, S., 2009, "Prediction of Acoustic Scattering in the Time Domain and Its Applications to Rotorcraft Noise," Ph.D. dissertation, Department of Aerospace Engineering, The Pennsylvania State University.

24 Sijtsma, P., 2007, "CLEAN based on spatial source coherence," International Journal of Aeroacoustics, Vol. 6, No. 4.

© 2018 Tecplot, Inc. All rights reserved worldwide. Tecplot®, Tecplot 360™ and the Tecplot 360™ Logo are registered trademarks and "Master the View™" is a trademark of Tecplot, Inc., Bellevue, WA, USA. All other trademarks are the property of their respective owners.